The Reason of Why Dynamic Dual-Energy CT is Better than Multi-Energy CT in Reducing Statistical Noise

Yidi Yao [a,b], Liang Li *[a,b], Zhiqiang Chen *[a,b]

[a] Department of Engineering Physics, Tsinghua University, Beijing 100084, China; [b] Key Laboratory of Particle and Radiation Imaging, Tsinghua University, Ministry of Education, Beijing 100084, China

ABSTRACT

Multi-energy CT conducted by photon-counting detectors has a wide range of applications, especially in multiple contrast agent imaging. However, multi-energy CT imaging suffers from higher statistical noise because of increased energy bin numbers. Our team has proposed the dynamic dual-energy CT imaging mode and the corresponding iterative imaging algorithms to solve this problem. The multi-energy projections and reconstructions calculated from the dynamic dual-energy CT data are less noisy than the static multi-energy CT, which has been verified by sufficient numerical simulations and experiments. However, a rigorous mathematical derivation has not been conducted to explain why dynamic dual-energy CT is better than static multi-energy CT in reducing statistical noise. In this work, we drive the noise model of the dynamic dual-energy CT to explain the reason. The reason is: compared to the multi-energy projections that are directly measured from a static multi-energy CT, the multi-energy projections, which are calculated from the dynamic dual-energy CT data, have the same expectation, but the variance is lower.

Keywords: spectral CT, multi-energy CT, CT reconstruction, photon-counting CT, dynamic dual-energy

1. INTRODUCTION

Photon-counting CT has made significant progress in both technique and clinical application in recent years[1]. Compared to energy-integrating CT, photon-counting CT has advantages in spatial resolution, radiation dose, equal weighting for all photons, etc. Multi-energy imaging is one of the major characteristics of photon counting CT, enabling simultaneous imaging of multiple contrast agents and the future of functional imaging. However, as the number of energy bins increases, the photon counts in each energy bin decrease, which leads to higher statistical noise of the projection data and bad quality of the reconstruction images.

To reconstruct less-noisy multi-energy CT images, we proposed the dynamic dual-energy (DDE) CT to reduce the statistical noise of the multi-energy CT data in our previous works [2-4]. The dual-energy CT data are obtained by applying an adjustable energy threshold in the photon-counting detector. The reconstruction and decomposition results calculated from the DDE CT data are less noisy than the static-energy-threshold multi-energy (SME) CT results, which have been verified through sufficient numerical simulations and experiments. However, why DDE CT outperforms SME CT in reducing statistical noise has not been explained in theory. Because DDE CT can utilize fewer data to reconstruct less-noisy multi-energy CT images is challengeable, giving a mathematical explanation is crucial to make DDE CT more acceptable.

In this work, we analyze DDE CT from the perspective of statistics. The mathematical foundation under DDE CT is: the variance of a Poisson random variable is larger than the variance of a random variable if this variable is calculated from a Poisson random variable with a larger expectation. Applying this principle to DDE CT, the conclusion is: if the ratios among the transmitted photons of different energy bins are accurately known, the noise of the multi-energy projections calculated from the DDE CT data is less than the noise of the multi-energy projections that are directly measured from the SME CT. With the convergence analysis of the simulation results, we further show that the ratios among the transmitted photons of different energy bins can be accurately calculated. In conclusion, we explain why DDE CT is better than SME CT in reducing statistical noise.

The structure of this paper is organized as follows. Since DDE CT is still a new concept, we first briefly review the DDE CT mode and the iterative DDE algorithm for multi-energy CT imaging in Section 2. Section 3 introduces the noise model of the DDE CT. Section 4 presents the convergence analysis of the DDE CT. Section 5 is the conclusion.Begin

the Introduction two lines below the Keywords. The manuscript should not have headers, footers, or page numbers. It should be in a one-column format. References are often noted in the text[1] and cited at the end of the paper.

2. REVIEW OF THE DYNAMIC DUAL-ENERGY CT

2.1 Dynamic Dual-Energy CT Mode

The SME CT diagram is shown in Figure 1a, and the DDE CT diagram is shown in Figure 1b. In SME CT, there are Nk energy thresholds for Nk-energy CT imaging. However, in DDE CT, there are only two energy thresholds. The low-energy threshold is unchanged and fixed, while the high-energy threshold changes among different preset values. When a photon is injected into the detector, it will be counted either in the low-energy bin or in the high-energy bin.

The high-energy thresholds change randomly for different detector pixels and different scan views. The preset values for the high-energy thresholds are set according to the requirement of multi-energy imaging. Nk-energy imaging requires Nk -1 preset values for the high-energy thresholds. These values are the same as the values of energy thresholds in an SME CT that aims for the same Nk-energy imaging.
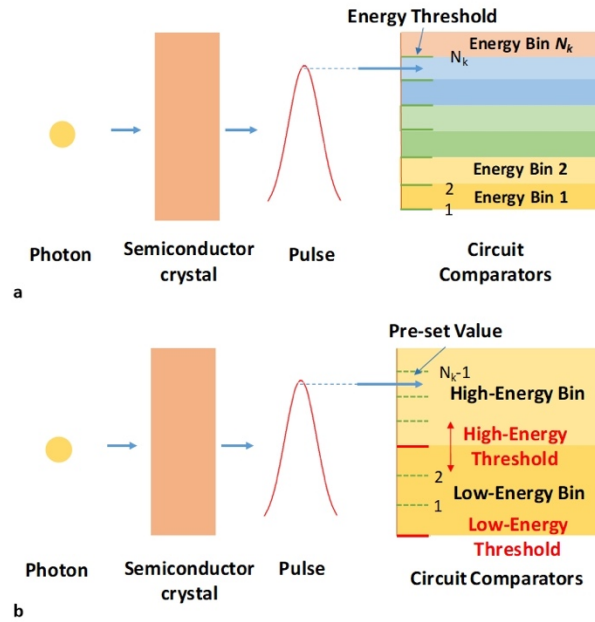
Figure 1. Diagrams of the SME CT (up) and DDE CT (down) [4].

2.2 Iterative Dynamic Dual-Energy CT Algorithm

In a DDE CT scan, there are two measurements $i_{low,j}$ and $i_{high,j}$ for the transmitted photons of the j_{th} ray. Supposing the measurements follow a Poisson distribution, the corresponding random variables of the measurements $I_{low,j}$ and $I_{high,j}$ are equal to:

$$I_{low,j} = Poisson\{\sum_{k=1}^{N_{th,j}} I_{0,k} \cdot \exp(-[A \cdot X_k]_j)\}$$

$$I_{high,j} = Poisson\{\sum_{k=N_{th,j}+1}^{N_k} I_{0,k} \cdot \exp(-[A \cdot X_k]_j)\}$$

(1)

In the above formula, $I_{0,k}$ are the incident photons of the k_{th}-energy bin, which is the same for all X-rays. $A \in {}^{N_j \times N_i}$ is the system matrix. N_j is the number of X-rays. N_i is the number of pixels in a reconstruction image. X_k is the accurate, noise-free reconstruction image of the k_{th} energy bin. $[AX_k]_j$ represents the line integral of the j_{th} X-ray. N_k is the number of total energy bins. $N_{th,j}$ is the number of preset values for the high-energy threshold at the j_{th} ray.

The iterative DDE CT algorithm for calculating the multi-energy projections from the DDE CT data can be concluded to the following two steps in one iteration:

Step 1: Update the multi-energy transmitted photons $\bar{i}_{k,j}$ using the last updated multi-energy CT results $\bar{X}_k$ and the low- and high-energy measurements $i_{low,j}$ and $i_{high,j}$.

Step 2: Update the multi-energy CT images $\bar{X}_k$ with the multi-energy transmitted photons $\bar{i}_{k,j}$.

For step 1, the multi-energy transmitted photons $\bar{i}_{k,j}$ can be calculated according to the following formula:

$$\bar{i}_{k,j} = \begin{cases} \dfrac{I_{0,k} \cdot \exp(-[A\bar{X}_k]_j)}{\sum\limits_{k=1}^{N_{th,j}} I_{0,k} \cdot \exp(-[A\bar{X}_k]_j)} \cdot i_{low,j}, & 1 \leq k \leq N_{th,j} \\[4mm] \dfrac{I_{0,k} \cdot \exp(-[A\bar{X}_k]_j)}{\sum\limits_{k=N_{th,j}+1}^{N_k} I_{0,k} \cdot \exp(-[A\bar{X}_k]_j)} \cdot i_{high,j}, & N_{th,j} < k \leq N_k \end{cases} \tag{2}$$

For step 2, the SIRT [5] algorithm is used for CT reconstruction of all energy bins. The initial values for the multi-energy CT image $\bar{X}_k$ are set to the values of the mono-energetic CT image, which can be reconstructed from the mono-energetic projections $i_{low,j} + i_{high,j}$.

3. THE NOISE MODEL OF DYNAMIC DUAL-ENERGY CT

3.1 The Property of Poisson Random Variable

In this section, we first discuss a property of the Poisson random variable. Considering a Poisson random variable X, the probability density function for the random variable X is:

$$P(X = k) = \frac{\lambda^k e^{-k}}{k!} \tag{3}$$

According to (3), the expectation and variance of the random variable X are equal to:

$$E(X) = \sum_{k=0}^{\infty} k \cdot \frac{\lambda^k e^{-k}}{k!} = \lambda \tag{4}$$

$$\begin{aligned} Var(X) &= E(X^2) - (E(X))^2 \\ &= \sum_{k=0}^{\infty} k^2 \cdot \frac{\lambda^k e^{-k}}{k!} - \lambda^2 \\ &= \lambda(\lambda+1) - \lambda^2 = \lambda \end{aligned} \tag{5}$$

Consider another Poisson random variable Y, where the expectation of Y is $t\lambda$ ($0 < t < 1$). According to (4) and (5), the expectation and variance of Y are:

$$E(Y) = Var(Y) = t\lambda \tag{6}$$

Consider a new random variable Z. Its definition is:

$$Z = tX, \quad 0 < t < 1 \tag{7}$$

The probability density function for Z is:

$$P(Z = tk) = \frac{\lambda^k e^{-k}}{k!} \tag{8}$$

The expectation and variance of Z are:

$$E(Z) = \sum_{k=0}^{\infty} tk \cdot \frac{\lambda^k e^{-k}}{k!} = t\lambda \tag{9}$$

$$D(Z) = E(Z^2) - (E(Z))^2$$
$$= \sum_{k=0}^{\infty} t^2 k^2 \cdot \frac{\lambda^k e^{-k}}{k!} - t^2 \lambda^2$$
$$= t^2 \lambda(\lambda+1) - t^2 \lambda^2 \qquad (10)$$
$$= t^2 \lambda$$

Random variables Y and Z have the same expectation, while the variance of Z is smaller than the variance of Y. The conclusion for the above derivation is: the variance of a Poisson random variable (Y) is larger than the variance of a random variable (Z), if this variable (Z) is calculated from the Poisson random variable with a larger expectation (X).

3.2 The Noise Model of Dynamic Dual-Energy CT

In this section, we drive the noise model of the DDE CT data and compare it to the SME CT data. Considering an N_k-energy SME CT, the number of transmitted photons in the k_{th}-energy bin I_k is a Poisson random variable. The number of transmitted photons of all energy bins I_{total} is also a Poisson random variable, and they satisfy the following relationship:

$$I_{total} = \sum_{k=1}^{N_k} I_k \qquad (11)$$

Therefore, the expectations of these random variables satisfy the following relationship:

$$E[I_k] = t_k \cdot E[I_{total}], \text{ where } 0 < t_k \leq 1, \sum_k t_k = 1 \qquad (12)$$

If the expectation of the number of total transmitted photons is λ_0, according to (6), the expectations and variances for the number of transmitted photons in different energy bins are:

$$E[I_k] = Var[I_k] = t_k \cdot \lambda_0 \qquad (13)$$

Now consider the DDE CT data. In DDE CT, the number of transmitted photons of the low-energy bin and the high-energy bin I_{low} and I_{high} are Poisson random variables and satisfy the following relationships:

$$I_{total} = I_{low} + I_{high} \qquad (14)$$

$$I_{low} = \sum_{k=1}^{N_{th}} I_k$$
$$I_{high} = \sum_{k=N_{th}+1}^{N_k} I_k \qquad (15)$$

Because the number of transmitted photons measured in the low-energy bin and the high-energy bin in a DDE CT are Poisson random variables, according to (13) and (15), their expectations and variations are equal to:

$$E[I_{low}] = Var[I_{low}] = (\sum_{k=1}^{N_{th}} t_k) \cdot \lambda_0$$
$$E[I_{high}] = Var[I_{high}] = (\sum_{k=N_{th}+1}^{N_k} t_k) \cdot \lambda_0 \qquad (16)$$

In DDE CT, the number of transmitted photons of multiple energy bins is not obtained from direct measurement but is calculated from the low- and high-energy bin data:

$$\bar{I}_k = \begin{cases} \dfrac{t_k}{\sum_{k=1}^{N_{th}} t_k} \cdot I_{low}, & 1 \leq k \leq N_{th} \\[4mm] \dfrac{t_k}{\sum_{k=N_{th}+1}^{N_k} t_k} \cdot I_{high}, & N_{th} < k \leq N_k \end{cases} \qquad (17)$$

$\bar{I}_k$ is still a random variable and represents the number of transmitted photons of the k_{th} energy bin. According to (9), (10), and (16), the expectation and variance of $\bar{I}_k$ are:

$$\mathrm{E}[\bar{I}_k] = t_k \cdot \lambda_0 \tag{18}$$

$$\mathrm{Var}[\bar{I}_k] = \begin{cases} t_k \cdot \dfrac{t_k}{\sum_{k=1}^{N_{th}} t_k} \cdot \lambda_0, & 1 \le k \le N_{th} \\[3mm] t_k \cdot \dfrac{t_k}{\sum_{k=N_{th}+1}^{N_k} t_k} \cdot \lambda_0, & N_{th} < k \le N_k \end{cases} \tag{19}$$

Comparing the expectation and variance of the number of multi-energy transmitted photons in SME CT and DDE CT, we can obtain the following relationship:

$$\mathrm{E}[\bar{I}_k] = \mathrm{E}[I_k] \tag{20}$$

$$\mathrm{Var}[\bar{I}_k] = \begin{cases} \dfrac{t_k}{\sum_{k=1}^{N_{th}} t_k} \cdot \mathrm{Var}[I_k], & 1 \le k \le N_{th} \\[3mm] \dfrac{t_k}{\sum_{k=N_{th}+1}^{N_k} t_k} \cdot \mathrm{Var}[I_k], & N_{th} < k \le N_k \end{cases} \tag{21}$$

For all k, the following inequalities always satisfy:

$$\frac{t_k}{\sum_{k=1}^{N_{th}} t_k} < 1, \quad \frac{t_k}{\sum_{k=N_{th}+1}^{N_k} t_k} < 1 \tag{22}$$

Therefore, we obtain the following conclusion: compared to the multi-energy CT transmitted photons I_k that are directly measured from an SME CT, the multi-energy transmitted photons $\bar{I}_k$, which are calculated from the DDE CT data, have the same expectation, but the variance is lower.

3.3 Verification

To verify the theory proposed in Section 3B, we simulate a large amount of data. We calculate the variances of the multi-energy CT transmitted photons for these simulation results and verify whether the relationship between the variances of the SME CT and the DDE CT is consistent with the theory.

A 20 cm diameter water cylinder is scanned in the simulation. The number of energy bins is 8. The variance images of the third-energy-bin SME CT transmitted photons and the third-energy-bin DDE CT transmitted photons are calculated from 1000 samples and shown in Figures 2a and 2b, respectively. If the proposed theory is correct, the following formula should be satisfied:

$$\mathrm{Ratio}_{k,j} \cdot \mathrm{Var}[prj_{k,j}] / \mathrm{Var}[\overline{prj}_{k,j}] = 1,$$

$$\text{where } \mathrm{Ratio}_{k,j} = \begin{cases} \dfrac{t_{k,j}}{\sum_{k=1}^{N_{th,j}} t_{k,j}}, & 1 \le k \le N_{th,j} \\[3mm] \dfrac{t_k}{\sum_{k=N_{th,j}+1}^{N_k} t_{k,j}}, & N_{th,j} < k \le N_k \end{cases} \tag{23}$$

k is the number of energy bins. j is the number of X-rays. The ratio image of the third energy bin is shown in Figure 2c. The third-energy bin calculation results are shown in Figure 2d. The mean value of Figure 2d is 1.0022, which is extremely close to 1. This result verifies the correctness of the noise model proposed in Section 3B.
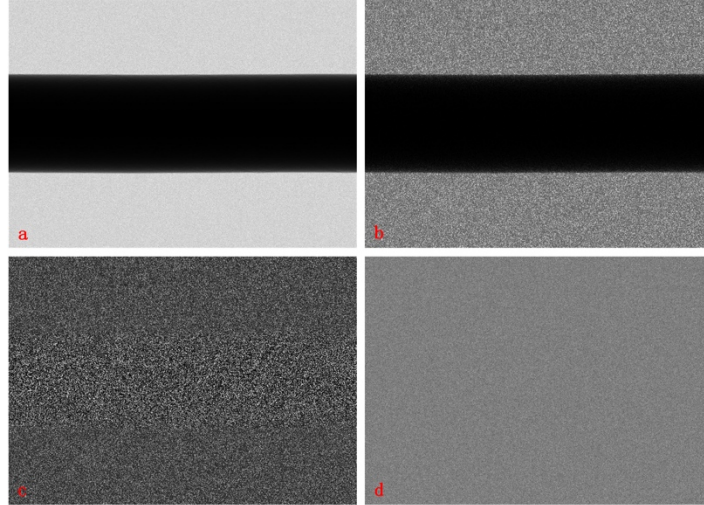
Figure 2. The variance images and calculation results of the third energy bin. 2a and 2b are variance images of the SME CT and DDE CT, respectively. 2c is the ratio image. 2d is the calculation result. The display windows for 2d is [0.5, 1.5].

4. THE NOISE MODEL OF DYNAMIC DUAL-ENERGY CT

4.1 Calculating Accurate t_k in the Dynamic Dual-Energy CT

Section 3 proves that the noise of projection calculated from DDE CT is lower than that calculated from SME CT. However, there is a premise for this conclusion: the ratios between the number of transmitted photons of a specific energy bin and all energy bins are accurately known, e.g., t_k is known and accurate for any k. In theory, t_k can be accurately calculated only if the noise-free transmitted photons of different energy bins are known. t_k cannot be calculated directly from the original DDE CT data.

The iterative DDE CT algorithm, which is described in Section 2B, is proposed to calculate accurate t_k. When the algorithm converges, (2) will be rewritten as:

$$\bar{i}_{k,j,converge} = \begin{cases} \dfrac{t_{k,j}}{\sum_{k=1}^{N_{th,j}} t_{k,j}} \cdot i_{low,j}, & 1 \le k \le N_{th,j} \\ \dfrac{t_{k,j}}{\sum_{k=N_{th,j}+1}^{N_k} t_{k,j}} \cdot i_{high,j}, & N_{th,j} < k \le N_k \end{cases}, \quad t_{k,j} = \dfrac{E[I_{k,j}]}{\sum_{k=1}^{N_k} E[I_{k,j}]} \tag{24}$$

$\bar{i}_{k,j,converge}$ is the convergent value for the multi-energy transmitted photons calculated from DDE CT and is an observation of the random variable defined in (17). Therefore, according to the conclusion in Section 3B, $\bar{i}_{k,j,converge}$ has lower statistical noise than $i_{k,j}$, which is the transmitted photon measured from the SME CT. In other words, the multi-energy projections calculated from the DDE CT data are less noisy than the SME CT if the iterative DDE algorithm converges.

4.2 Convergence of the Iterative Dynamic Dual-Energy Algorithm

The convergence of the iterative DDE algorithm is verified through simulation. The XCAT thorax phantom [6] is scanned in the simulation. The simulation configurations are shown in Table 1.

Table 3. Configuration of the simualtion

Item Parameter	Video Value
Scan Method	2D fan-beam
Source Voltage	120 kV
Distance between Source and Detector	100 cm
Distance between Source and Gantry Center	50 cm
Views over 360 Degrees	720
Number of Detectors	1024
Detector Length	1 m
Size of Reconstruction Image	512 * 512
Reconstruction Pixel Size	1 mm * 1 mm
Number of Energy Bins	8
Number of Incident Photons for Each Ray	$5*10^6$

The noise of the projections is measured in terms of the relative error, which is defined as:

$$\text{RelativeError}(prj) = \frac{\|prj - prj_{truth}\|^2}{\|prj_{truth}\|^2} \times 100\% \tag{25}$$

prj_{truth} is the ground truth of the line integrals of multi-energy CT, which can be obtained from the noise-free SME CT. In the analysis of the convergence, the relative error is calculated for line integrals of three types: the multi-energy line integrals measured in SME CT, the multi-energy line integrals calculated from DDE CT data, and the convergent values for the multi-energy line integrals from DDE CT. If the algorithm converges, the second type of relative error will decrease to the same value as the third type of relative error.

The convergence curve is plotted in Figure 3, which shows that the algorithm converges. This illustrates that the iterative DDE algorithm can accurately calculate t_k. Moreover, the relative errors of the multi-energy line integrals from the DDE CT are much smaller than the relative errors of the multi-energy line integrals from the SME CT, which indicates that a less-noisy multi-energy projection can be calculated from the DDE CT.
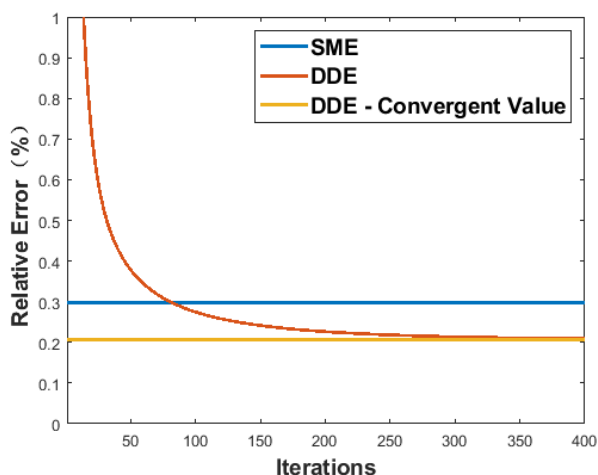
Figure 3. The convergence curve.

5. CONCLUSION

In this work, we derive the noise model of DDE CT to explain why DDE CT can reduce statistical noise better than SME CT. Based on this derivation, we further analyze the convergence of DDE CT and show that the multi-energy projection calculated from DDE CT is less noisy than that calculated from SME CT.

REFERENCES

[1] M. Danielsson, M. Persson, and M. Sjolin, "Photon-counting x-ray detectors for CT," Phys. Med. Biol., vol. 66, no. 3, Feb 7 2021, Art no. 03tr01, doi: 10.1088/1361-6560/abc5a5.

[2] L. Li, Z. Chen, W. Cong, and G. Wang, "Spectral CT modeling and reconstruction with hybrid detectors in dynamic-threshold-based counting and integrating modes," Ieee T Med Imaging, vol. 34, no. 3, pp. 716-728, 2015.

[3] Y. D. Yao, L. Li, and Z. Q. Chen, "Dynamic-dual-energy spectral CT for improving multi-material decomposition in image-domain," (in English), Phys. Med. Biol., Article vol. 64, no. 13, p. 22, Jul 2019, Art no. 135006, doi: 10.1088/1361-6560/ab196d.

[4] Y. Yao, L. Li, and Z. Chen, "Iterative dynamic dual-energy CT algorithm in reducing statistical noise in multi-energy CT imaging," Physics in Medicine & Biology, 2021. [Online]. Available: http://iopscience.iop.org/article/10.1088/1361-6560/ac459d.

[5] J. Gregor and T. Benson, "Computational analysis and improvement of SIRT," Ieee T Med Imaging, vol. 27, no. 7, pp. 918-924, Jul 2008, doi: 10.1109/tmi.2008.923696.

[6] W. P. Segars, G. Sturgeon, S. Mendonca, J. Grimes, and B. M. W. Tsui, "4D XCAT phantom for multimodality imaging research," (in English), Medical Physics, Article vol. 37, no. 9, pp. 4902-4915, Sep 2010, doi: 10.1118/1.3480985.